Louisiana State University

LSU Digital Commons

6-4-2013

Interplay between superconductivity and magnetism in Fe 1-xPdxTe

Amar B. Karki
Louisiana State University

V. Ovidiu Garlea
Oak Ridge National Laboratory

Radu Custelcean
Oak Ridge National Laboratory

Shane Stadler
Louisiana State University

E. W. Plummer
Louisiana State University

See next page for additional authors

Recommended Citation

Authors

Amar B. Karki, V. Ovidiu Garlea, Radu Custelcean, Shane Stadler, E. W. Plummer, and Rongying Jin

Interplay between superconductivity and magnetism in Fe$_{1-x}$Pd$_x$Te

Amar B. Karki[a], V. Ovidiu Garlea[b], Radu Custelcean[c], Shane Stadler[a], E. W. Plummer[a,1], and Rongying Jin[a,1]

[a]Department of Physics and Astronomy, Louisiana State University, Baton Rouge, LA 70803; and [b]Quantum Condensed Matter Division and [c]Chemical Science Division, Oak Ridge National Laboratory, Oak Ridge, TN 37831

The attractive/repulsive relationship between superconductivity and magnetic ordering has fascinated the condensed matter physics community for a century. In the early days, magnetic impurities doped into a superconductor were found to quickly suppress superconductivity. Later, a variety of systems, such as cuprates, heavy fermions, and Fe pnictides, showed superconductivity in a narrow region near the border to antiferromagnetism (AFM) as a function of pressure or doping. However, the coexistence of superconductivity and ferromagnetic (FM) or AFM ordering is found in a few compounds [RRh$_4$B$_4$ (R = Nd, Sm, Tm, Er), R′Mo$_6$X$_8$ (R′ = Tb, Dy, Er, Ho, and X = S, Se), UMGe (M = Ge, Rh, Co), CeCoIn$_5$, EuFe$_2$(As$_{1-x}$P$_x$)$_2$, etc.], providing evidence for their compatibility. Here, we present a third situation, where superconductivity coexists with FM and near the border of AFM in Fe$_{1-x}$Pd$_x$Te. The doping of Pd for Fe gradually suppresses the first-order AFM ordering at temperature $T_{N/S}$, and turns into short-range AFM correlation with a characteristic peak in magnetic susceptibility at $T′_N$. Superconductivity sets in when $T′_N$ reaches zero. However, there is a gigantic ferromagnetic dome imposed in the superconducting-AFM (short-range) cross-over regime. Such a system is ideal for studying the interplay between superconductivity and two types of magnetic (FM and AFM) interactions.

Since the first discovery of superconductivity (SC) a century ago, the effects of magnetic impurities and the possibility of magnetic ordering in superconductors has been a central topic of condensed matter physics. Due to strong spin scattering (1, 2), it has generally been believed that the conduction electrons cannot be both magnetically ordered and superconducting. Even though it is thought that Cooper pairs in cuprates, heavy fermions, and Fe-based compounds are mediated by spin fluctuations (3–5), SC generally occurs after suppressing the magnetic ordering either through chemical doping or the application of hydrostatic pressure (6–10). However, there is growing evidence for the coexistence of superconductivity with either ferromagnetic (FM) (11–20) or antiferromagnetic (AFM) ordering (21–24). With the decrease of temperature (T), some of these systems show magnetic ordering before the superconducting transition (T_c) (14–17, 20), some are ordered in a reversed sequence (11–13, 18, 19, 22), some have the two orderings occur concomitantly (22, 25), and some show reentrant superconductivity (partially) overlapping with a magnetically ordered phase (11–13, 26). Despite extensive investigations of interaction between SC and magnetic moments, there is so far no unified theory for the coexistence of SC and magnetism. With the lack of theoretic guidance, the existing experimental findings lead to two schools of thought: one is that both orders result from the same conduction electrons as evidenced by their synchronized magnetic and superconducting orders (22), and the other is that there are two separate sets of electrons responsible for magnetic ordering and superconductivity, respectively (19, 21, 25). What remains incomprehensible is the case where superconductivity and magnetic ordering coexist but are in competition with each other, as seen in Fe-based systems (23, 24, 27).

The discovery of superconductivity in Fe-based compounds has sparked enormous interest in the scientific community. Although

Fe is the most well known ferromagnet, all parent compounds of Fe-based superconductors exhibit AFM ordering. Though superconductivity is induced after suppressing the AFM ordering, it can coexist with either remaining AFM ordering (23, 24, 27) or new FM ordering (18, 19), and this provides an ideal platform for studying the interplay between superconductivity and magnetism. Among the Fe-based superconductors, the chalcogenide FeTe$_{1-x}$Se$_x$ is unique in several aspects: (*i*) it is the only compound composed of slabs of Fe(Te/Se)$_4$ stacked together without an interlayer spacer; (*ii*) it becomes superconducting via isovalent doping of Se for Te, with the highest T_c occurring at the 50% doping level; and (*iii*) the parent compound Fe$_{1+y}$Te shows nonmetallic electrical conduction and forms (π, π)-type AFM ordering with a large magnetic moment (28, 29), in contrast to the (π, 0)-type ordering with a small magnetic moment seen in Fe pnictides. The unusual AFM order in Fe$_{1+y}$Te cannot be explained by a simple Fermi-surface nesting picture, thus leading to arguments for a correlated local-moment scenario (27). Because of these differences, the application of hydrostatic pressure or partial doping on the Fe site, such as with Co or Ni, does not generate the generic phase diagram as seen for other Fe-based superconductors (30–33).

To gain insight into the relationship between magnetism and superconductivity, we choose to substitute Pd for Fe in FeTe. This decision is motivated by the following: (*i*) Pd is known to exhibit FM instability (34, 35) even though it is paramagnetic in bulk, and (*ii*) PdTe is a superconductor with T_c ∼4.5 K (36–42). The partial replacement of Fe by Pd will allow us to understand the roles of Fe, Pd, and Te in both magnetism and superconductivity. Based on electrical transport, and magnetic and thermodynamic property measurements, we show that the ground state of Fe$_{1-x}$Pd$_x$Te varies from AFM to FM ordering, to a superconducting state; this is one of rare cases where superconductivity flirts with both AFM and FM.

Single crystals of Fe$_{1-x}$Pd$_x$Te were grown via high-temperature melting, with the procedure described in *SI Text*. The crystal structure and the phase purity were measured by both powder and single-crystal X-ray diffraction. Fig. 1 shows powder X-ray diffraction patterns (Fig. 1*A*) and lattice parameters obtained from single-crystal X-ray refinement (Fig. 1*B*) for different doping levels; it confirms that the undoped FeTe forms a tetragonal structure, belonging to the P4/*nmm* space group. At room temperature, the lattice parameters are a = 3.8202 Å and c = 6.2686 Å. Similar to previous observations (43), our single-crystal refinement result indicates that there are ∼9% extra Fe atoms (T2 site of Fig. 1*B*) incorporated at interstitial sites of
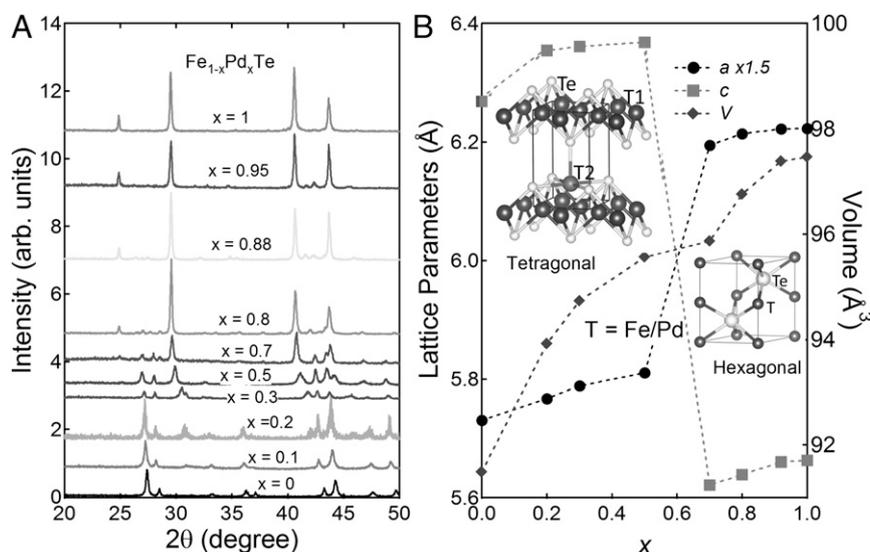
PHYSICS

Fig. 1. $Fe_{1-x}Pd_xTe$: (*A*) Powder X-ray diffraction patterns and (*B*) its unit cell parameters at room temperature obtained from single-crystal X-ray refinement.

the Te layers. As soon as Pd is introduced into the system, the interstitial sites of $Fe_{1-x}Pd_xTe$ are occupied by Pd atoms (i.e., T2 = Pd when $x > 0$); though it remains in the same tetragonal space group, its lattice parameters a and c both increase with increasing Pd doping concentration for $x \leq x_s \sim 0.6$ (Fig. 1*B*). This finding indicates that Pd doping creates negative pressure, which is surprising because Pd^{2+} (~0.80 Å) has a nearly identical ionic radius as that of Fe^{2+} (~0.77 Å). The crystal structure of $Fe_{1-x}Pd_xTe$ remains tetragonal up to x_s (~0.6). Above x_s, $Fe_{1-x}Pd_xTe$ crystallizes in a hexagonal structure (space group $P6_3/mmc$), and its lattice parameters also increase with increasing x (Fig. 1*B*); this results in an increase of the unit cell volume with increasing x in the entire doping range (Fig. 1*B*). In the hexagonal structure, the system no longer incorporates any interstitial sites (Tables S1–S4). Though the hexagonal structure at $x > x_s$ can be regarded as a deformed FeTe structure, the local environment of Fe/Pd is transformed from a tetrahedron ($x < x_s$) to an octahedron ($x > x_s$) (44).

To correlate the structural information with physical properties, we show, in Fig. 2, the doping dependence of structural,
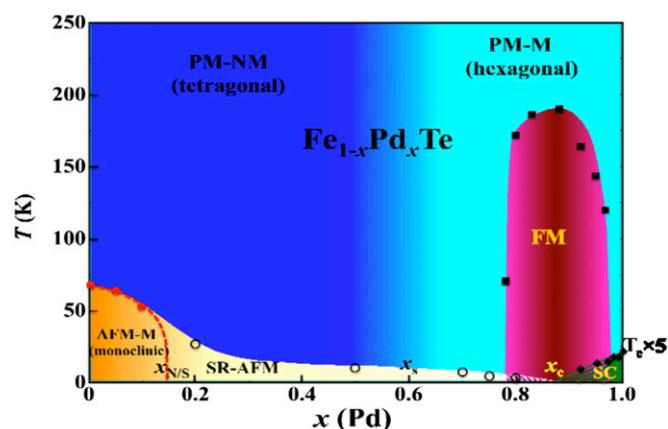
electrical, and magnetic properties of $Fe_{1-x}Pd_xTe$, with specifics presented later. The undoped ($x = 0$) $Fe_{1.09}Te$ undergoes both an AFM ordering and a structural transition from paramagnetic (PM) tetragonal (high temperatures) to an AFM-ordered monoclinic (low temperatures) phase at $T_{N/S} \sim 70$ K, with the first-order characteristic. Upon Pd doping, $T_{N/S}$ is suppressed (solid circles), reaching zero at $x = x_{N/S} \sim 0.15$ (dash line). In this doping region, the electrical resistivity (ρ) changes from nonmetallic (NM) character ($d\rho/dT < 0$) above $T_{N/S}$ to metallic (M) behavior ($d\rho/dT > 0$) below $T_{N/S}$. When the characteristic feature for the first-order transition is absent at $x_{N/S}$, the magnetic susceptibility of $Fe_{1-x}Pd_xTe$ exhibits a peak at T'_N. The value of T'_N decreases with increasing x (Fig. 2, open circles), which eventually reaches zero at $x_c \sim 0.88$. The magnetic susceptibility peak is a signature for short-range (SR) AFM correlation developed below T'_N, with no obvious fingerprint in the electrical resistivity. Above x_c, superconductivity appears (Fig. 2, solid diamonds). The transition temperature T_c increases with increasing x. Remarkably, the system shows ferromagnetism (Fig. 2, solid squares) in the doping range of $0.78 \leq x \leq 0.98$ with the maximum T_{FM} (~190 K) at x_c, where AFM and SC vanish. In addition to the variable magnetic phases, there is doping-induced structural phase transition, being tetragonal at $x < x_s \sim 0.6$ (Fig. 2, dark blue) and hexagonal at $x > x_s$ (light blue). Such a structural transition is responsible for a change of electronic structure, manifested by NM behavior at $x < x_s$ and a metallic character at $x > x_s$.

We now present the detailed experimental results in support of the phase diagram. Fig. 3*A* shows the temperature dependence of ρ of $Fe_{1-x}Pd_xTe$ for $0 \leq x \leq 0.5$ (the experimental technique is described in *SI Text*). Similar to previous observations (45), the electrical resistivity of undoped ($x = 0$) $Fe_{1.09}Te$ increases with decreasing temperature at high temperatures, but sharply decreases below $T_{N/S} \sim 70$ K; this is caused by the first-order coupled structural and AFM phase transition (45, 46). Below $T_{N/S}$, the structure of $Fe_{1.09}Te$ becomes monoclinic. Upon Pd doping, $T_{N/S}$ is suppressed, and the first-order transition is no longer observed at $x = 0.2$. The smooth and monotonic temperature dependence of ρ indicates the absence of both structural and AFM transitions at $0.1 < x < 0.2$. Though it sustains a nonmetallic temperature dependence ($d\rho/dT < 0$) down to 2 K, the magnitude of the electrical resistivity deceases with increasing x in the entire doping range above $T_{N/S}$ (Fig. 3 *A* and *C*). For $0.5 < x \leq 1.0$, the electrical resistivity of $Fe_{1-x}Pd_xTe$ continues to decrease with increasing x, as shown in Fig. 3*B*.

Fig. 2. Phase diagram of $Fe_{1-x}Pd_xTe$. AFM, antiferromagnetic; AFM-M, antiferromagnetically ordered metallic state; FM, ferromagnetically ordered state; M, metallic; NM, nonmetal; PM, paramagnetic; PM-M, paramagnetic metal; SC, superconductivity; SR, short-range; SR-AFM, short-range AFM correlation.
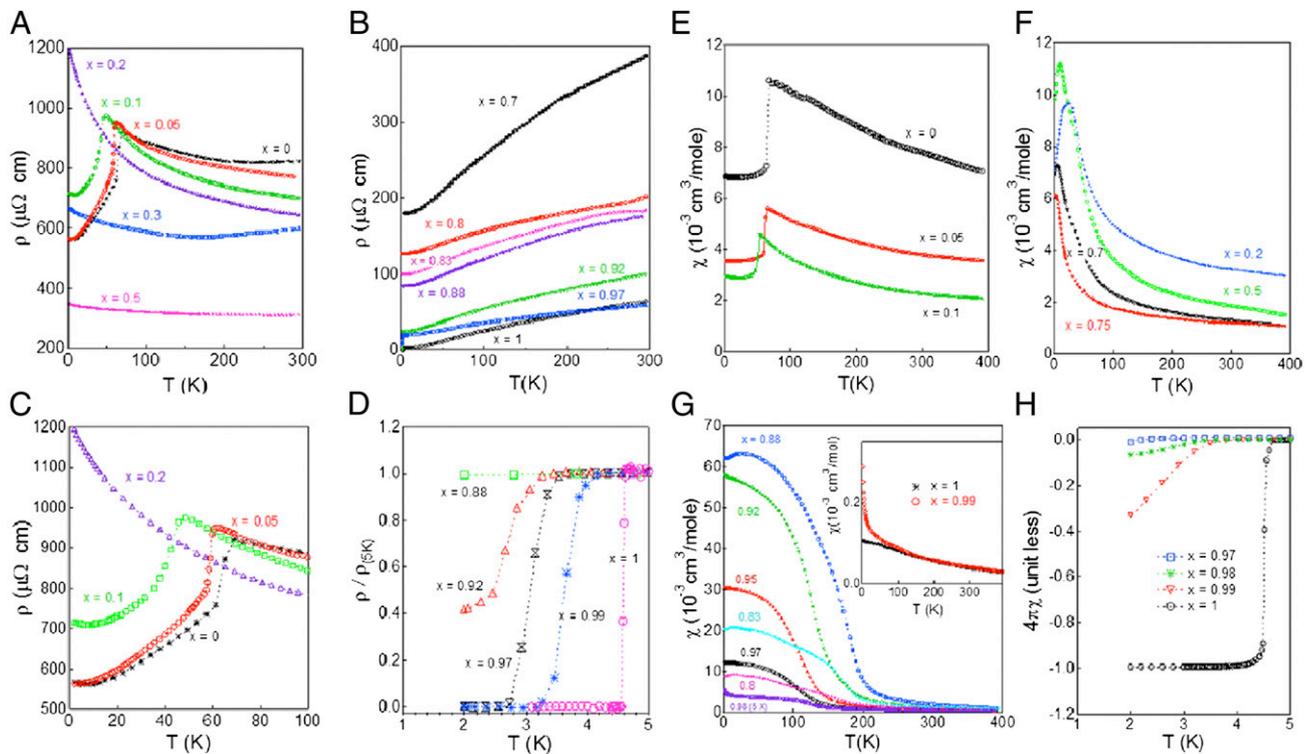
Karki et al.

Fig. 3. (*A* and *B*) Temperature dependence of the electrical resistivity (ρ) of $Pd_{1-x}Fe_xTe$ at the indicated compositions. (*C* and *D*) Temperature dependence of ρ near the first-order AFM/structural transition in the low-doping region, and the superconducting transition in the high-doping region plotted as $\rho/\rho(5\ K)$ vs. T, respectively. (*E–G*) Temperature dependence of the magnetic susceptibility (χ) of $Fe_{1-x}Pd_xTe$ measured at a magnetic field of 1 T. *G Inset* shows χ vs. $x = 0.99$ and 1.0; *H* is the $\chi(T)$ measured at 20 oersted (Oe) for $0.97 \leq x \leq 1.0$.

More interesting is that ρ shows metallic behavior ($d\rho/dT > 0$) in the entire temperature range measured for $0.5 < x \leq 1.0$. We believe that the cross-over from nonmetallic to metallic character is associated with the structural change at x_s. Furthermore, there is a sharp drop of resistivity at low temperatures for $0.88 < x \leq 1.0$, as shown in Fig. 3D. This drop is due to the emergence of superconductivity because the magnetic susceptibility shows diamagnetism as well in the temperature range (Fig. 3H). Note that the superconducting transition temperature T_c increases with increasing x.

With Pd doping, the magnetic properties of $Fe_{1-x}Pd_xTe$ also change. Fig. 3 *E–H* shows the temperature dependence of the magnetic susceptibility, χ, at indicated values x. For $0 \leq x < 0.2$, χ initially increases with decreasing temperature, and then drops steeply at $T_{S/N}$ (Fig. 3E); this confirms the first-order nature of the structural/AFM transition at $0 \leq x < 0.2$. Such a feature is absent for $x \geq x_{N/S} \sim 0.15$. Instead, there is a characteristic peak in magnetic susceptibility at T'_N (Fig. 3F). Because there is no anomaly in electrical resistivity (Fig. 3 *A–C*) or specific heat, the susceptibility peak cannot be due to a true phase transition, but rather marks the onset of SR AFM correlation as seen in other materials (47). With increasing x, T'_N moves to lower temperatures, and the magnitude of χ decreases as well (Fig. 3F). Though the characteristic peak is expected to completely vanish around $x = x_c \sim 0.88$, the magnetic susceptibility reveals a dramatic increase below another characteristic temperature T_{FM} at $x \geq 0.78$, as shown in Fig. 3G, which indicates the onset of ferromagnetic ordering at T_{FM}. With increasing x, T_{FM} initially increases then decreases after reaching the maximum (~ 190 K) at $x = x_c \sim 0.88$. Interestingly, the low-temperature susceptibility peak is still present for samples with $x = 0.78$, 0.80, 0.83, and 0.88, which suggests the coexistence of FM ordering and AFM interactions in this doping region. Above x_c, $\chi(T)$ continues to

show FM behavior at high temperatures, but becomes negative at low temperatures (below T_c) under low magnetic fields, as depicted in Fig. 3H. The negative χ below T_c indicates the emergence of superconductivity, because their electrical resistivities also drop sharply (Fig. 3D). Whereas T_{FM} decreases, T_c increases with increasing x (above x_c). As shown Fig. 3G Inset, $\chi(T)$ exhibits paramagnetic behavior above T_c for $x = 0.99$ and 1.0, indicating the complete suppression of FM. However, T_c continues to increase with x (Fig. 3H).

Clearly, there is a coexistence of AFM and FM ordering at $0.78 \leq x \leq 0.88$, and of FM ordering and SC at $0.88 \leq x \leq 0.98$ at low temperatures for $Fe_{1-x}Pd_xTe$, which is further supported by the following results. First, the high-temperature magnetic susceptibility data allows us to extract both Curie–Weiss temperature (θ_{CW}) and effective magnetic moment (μ_{eff}) by fitting our experimental data to the Curie–Weiss law $\chi(T) = \chi_0 + \frac{N_A \mu_{eff}^2}{3k_B(T - \theta_{CW})}$, where N_A is the Avogadro's constant and k_B is Boltzmann's constant. The x dependences of θ_{CW} and μ_{eff} are shown in Fig. 4 *A* and *B*, respectively. Note that $\theta_{CW} < 0$ for $x \leq 0.8$, indicating that the dominant magnetic interaction is AFM in this doping region. The fact that $|\theta_{CW}| \gg T_{N/S}$ implies 2D AFM ordering for $x < 0.2$, whereas a small θ_{CW} value at $0.2 \leq x \leq 0.8$ is consistent with our interpretation that there is short-range AFM correlation. And $\theta_{CW} > 0$ for $0.8 \leq x < 0.98$, which confirms the ferromagnetic interaction in this doping range. Although θ_{CW} is comparable to the corresponding transition temperature T_{FM}, the effective magnetic moment is small, as shown in Fig. 4B, which implies that the FM ordering results mainly from Fe, even though Pd has to be the vehicle of coupling between Fe atoms (see discussion below). According to the single-crystal X-ray refinement results (Tables S1–S3), the actual Fe concentration is very close to the nominal value for $0.8 \leq x \leq 0.98$. We thus estimate the effective magnetic moment of Fe using the nominal Fe concentrations;
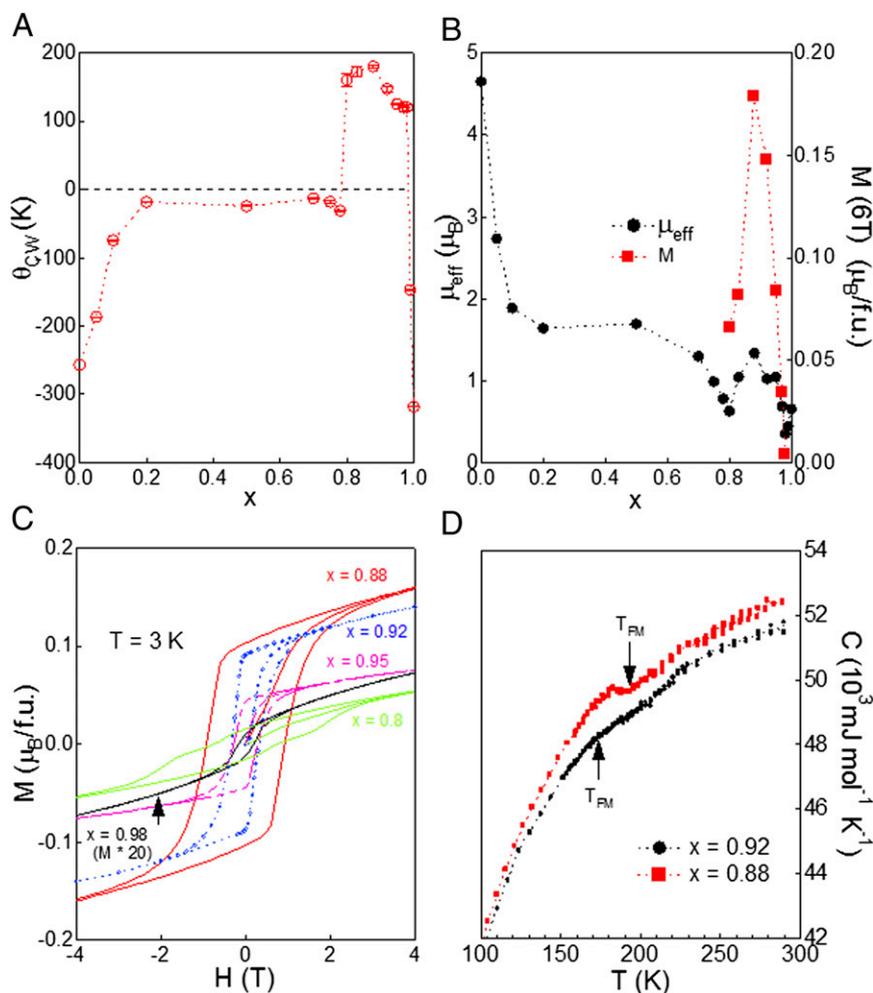
Fig. 4. Fe1-*x*Pd*x*Te (*A*) Doping dependence of Curie–Weiss temperature. (*B*) Doping dependence of the effective magnetic moment and magnetization at 6 T. (*C*) Magnetization vs. magnetic field at 3 K for *x* = 0.8, 0.88, 0.92, 0.95, and 0.98. (*D*) Specific heat vs. temperature for *x* = 0.92 and 0.88.

this gives $\mu_{eff} = 1.60\mu_B$/Fe ($x = 0.80$), $2.42\mu_B$/Fe ($x = 0.83$), $3.79\mu_B$/Fe ($x = 0.88$), $4.21\mu_B$/Fe ($x = 0.92$), $3.53\mu_B$/Fe ($x = 0.95$), and $2.52\mu_B$/Fe ($x = 0.98$). Note that the highest magnetic moment for $x = 0.92$ is close to the Fe moment in Fe$_{1.09}$Te ($\sim 4.65\mu_B$/Fe), as plotted in Fig. 4*B*. In the latter case, the actual ordered magnetic moment is $\sim 3.31\mu_B$/Fe (28), smaller than that obtained from the Curie–Weiss constant; this is explained as due to the itinerant nature of the electrons in FeTe (28). For Fe$_{1-x}$Pd$_x$Te, we may estimate the ordered magnetic moment from the magnetization. Fig. 4*C* shows the field dependence (*H*) of magnetization (M) at $T = 3$ K for *x* between 0.80 and 0.98. Note that M(*H*) reveals a well-defined hysteresis loop, confirming the nature of FM ordering for $0.8 \leq x \leq 0.98$. Though M(*H*) is not saturated up to 6 T, we may estimate the lower bound of the ordered magnetic moment using M($H = 6$ T) data shown in Fig. 4*B*. At $T = 3$ K, $\mu \sim 0.33\mu_B$/Fe ($x = 0.80$), $0.48\mu_B$/Fe ($x = 0.83$), $1.49\mu_B$/Fe ($x = 0.88$), $1.85\mu_B$/Fe ($x = 0.92$), $1.67\mu_B$/Fe ($x = 0.95$), and $0.22\mu_B$/Fe ($x = 0.98$). In addition to the fact that M ($H = 6$ T) < M$_{sat}$, the small ordered magnetic moment could result from (*i*) the itinerant nature of the electrons and (*ii*) the reduced concentration of Fe in the highly Pd doped region. Nevertheless, the specific heat reveals anomalies in the compounds with high T_{FM} (Fig. 4*D*), indicating a true phase transition at T_{FM}.

From the results presented here, it is most likely that the FM dome is intrinsic, due to the ordering of the Fe magnetic moments. Within the dome, our single-crystal X-ray refinement indicates

that the structure remains the same as that of pure PdTe with actual Fe concentration close to the nominal value, and there are no interstitial sites of either Pd or Fe, which strongly suggests that the FM ordering is not due to the formation of Fe clusters. In early studies, FM was detected in alloys of Fe in Pd (i.e., Pd$_{1-x}$Fe$_x$) at compositions down to 0.08% Fe (48), because magnetic moments on the Fe sites polarize the surrounding Pd matrix (48–51). It seems that Fe doping in PdTe compound gives rise to a similar effect, i.e., Pd matrix mediates the magnetic interactions between Fe atoms.

The central question is, how can both FM ordering and superconductivity coexist in the region of $0.88 \leq x \leq 0.98$? Having excluded the possibility of structural phase separation, one may consider the scenario of electronic phase separation with either macroscopic coexistence of singlet SC and FM in different regions or microscopic coexistence of triplet SC and FM (11, 21, 52). If Fe$_{1-x}$Pd$_x$Te were a triplet superconductor, a small amount of impurity or disorder would completely suppress superconductivity, as seen in Sr$_2$RuO$_4$ (53). Though we observe anomalous specific heat below T_c of PdTe (42), the insensitivity to Fe doping does not support triplet SC. For the former case, further experimental investigations are necessary, such as combined scanning electron microscopy and tunneling microscopy to directly probe both SC and FM regions. Theoretically, almost all Pd *d* orbitals in PdTe are occupied due to the covalency of the Pd–Te bonding, according to recent first-principle calculations (44), and this

leads to a strong suppression of the local magnetic moment (44). As shown in Fig. 3*G* (*Inset*), the magnetic susceptibility of PdTe ($x = 1$) indeed exhibits paramagnetic behavior above T_c. Upon substitution of Pd by Fe, T_c decreases nearly linearly with increasing Fe concentration ($1 − x$; Fig. 2). As Fe concentration reaches ~3% ($1 − x = 0.03$), both SC and FM ordering coexist. The fact that FM ordering does not immediately kill superconductivity is likely due to the unique electronic structure of PdTe. First-principles calculations indicate that the states in the proximity of the Fermi level consist mainly of Te *p* electrons, which are weakly hybridized with Pd e_g orbitals (44); this is in dramatic contrast to the electronic structure of FeTe, in which the states near the Fermi level derived from Fe with direct Fe–Fe interactions, and the Te *p* states lie well below the Fermi level and hybridized weakly with the Fe *d* states (54). For PdTe, the partial doping of Fe may lead to an even weaker hybridization between Te *p* and Pd e_g orbitals, due to the shift of Fermi level. Our experimental observation is in support of this scenario: with increasing Fe concentration, superconductivity is gradually suppressed to zero, at which the FM ordering reaches the maximum (Figs. 2 and 4). After T_c reaches zero at x_c, the disappearance of the superconducting energy gap allows the rearrangement of electronic structure, which is in favor of antiferromagnetic interaction; the latter apparently competes with the existing FM interaction, thus leading to the complete suppression of FM at $x < 0.78$.

In summary, the substitution of Fe by Pd results in an extremely rich phase diagram for $Fe_{1−x}Pd_xTe$. Powder and single-crystal X-ray diffraction measurements both indicate that there is doping-induced structural transition from a tetragonal phase at $x < x_s$ ~0.6 to a hexagonal phase at $x > x_s$. Correspondingly, the electrical resistivity changes from nonmetallic character at $x < x_s$ to metallic behavior at $x > x_s$. Magnetically, the system undergoes a first-order AFM transition at $T_{N/S}$ for $x \leq x_{N/S}$ ~0.15, with the structure transition occurring at the same temperature from tetragonal to monoclinic. When $T_{N/S}$ approaches zero at $x_{N/S}$, there is no longer a temperature-induced structural transition, whereas short-range AFM correlation exists for $x_{N/S} < x \leq 0.88$. Superconductivity sets in at $x \geq x_c$ ~0.88. In addition, a gigantic FM dome with $0.78 \leq x \leq 0.98$ is centered at the critical concentration x_c, where both AFM and SC vanish. The coexistence of FM ordering with either SR AFM or SC results most likely from the unique electronic structure of $Fe_{1−x}Pd_xTe$. With the low Pd concentration, both electrical conduction and magnetism of $Fe_{1−x}Pd_xTe$ are determined by Fe/Pd *d* electrons, because they are near the Fermi level. Due to the ferromagnetic instability and the extended orbitals of 4*d* electrons of Pd, both AFM interactions and electrical resistivity in $Fe_{1−x}Pd_xTe$ decrease with increasing *x*. Before the complete suppression of SR AFM, FM ordering occurs due to the Fe magnetic moment polarization in the Pd matrix. However, the hexagonal structure at $x > x_s$ with Pd/Fe in an octahedral environment leads to more localized *d* electrons from Pd/Fe but itinerant *p* electrons from Te. It seems that the weak hybridization between *p*–*d* electrons allows for the magnetic ordering of Fe/Pd moments and superconducting ordering of *p* conduction electrons. Nevertheless, these two orderings compete with each other. Hence, the physics of $Fe_{1−x}Pd_xTe$ in the hexagonal phase is in contrast to known Fe-based superconductors, in which physical properties are mainly determined by Fe *d* states. $Fe_{1−x}Pd_xTe$ provides another and rare example for studying the interplay between SC, FM, and AFM ordering, where two separate sets of electrons are responsible for FM ordering and superconductivity, respectively.

1. Maple MB (1976) Superconductivity—a probe of the magnetic state of local moments in metals. *Appl Phys (Berl)* 9(3):179–204.
2. Ginzburg VL (1957) Ferromagnetic superconductors. *Sov Phys JETP* 4:153–161.
3. Mathur ND, et al. (1998) Magnetically mediated superconductivity in heavy fermion compounds. *Nature* 394(6688):39–43.
4. Onufrieva F, Pfeuty P (2012) Low-doping anomalies in high-T_c cuprate superconductors as evidence of a spin-fluctuation-mediated superconducting state. *Phys Rev Lett* 109(25):257001.
5. Chubukov A (2012) Pairing mechanism in Fe-based superconductors. *Annual Rev Cond Matt Phys* 3:57–92.
6. Hüffner S, Hossain MA, Damascelli A, Sawatzky GA (2008) Two gaps make a high-temperature superconductor? *Rep Prog Phys* 71(6):062501.
7. Kamihara Y, Watanabe T, Hirano M, Hosono H (2008) Iron-based layered superconductor La[O$_{(1−x)}$F$_x$]FeAs (x = 0.05–0.12) with T(c) = 26 K. *J Am Chem Soc* 130(11):3296–3297.
8. Sefat AS, et al. (2008) Superconductivity at 22 K in Co-doped BaFe$_2$As$_2$ crystals. *Phys Rev Lett* 101(11):117004.
9. Mizuguchi Y, et al. (2010) Mössbauer studies on FeSe and FeTe. *Physica C* 470(Suppl 1):S338–S339.
10. Sales BC, et al. (2009) Bulk superconductivity at 14 K in single crystals of Fe$_{1+y}$Te$_x$Se$_{1−x}$. *Phys Rev B* 79(9):094521.
11. Fertig WA, et al. (1977) Destruction of superconductivity at the onset of long-range magnetic order in the compound ErRh$_4$B$_4$. *Phys Rev Lett* 38(17):987–990.
12. Ishikawa M, Fischer Ø (1977) Destruction of superconductivity by magnetic ordering in Ho$_{1.2}$Mo$_6$S$_8$. *Solid State Commun* 23(1):37–39.
13. Canfield PC, Bud'ko SL, Cho BK (1996) Possible co-existence of superconductivity and weak ferromagnetism in ErNi$_2$B$_2$C. *Physica C* 262(3-4):249–254.
14. Saxena SS, et al. (2000) Superconductivity on the border of itinerant-electron ferromagnetism in UGe$_2$. *Nature* 406(6796):587–592.
15. Huy NT, et al. (2007) Superconductivity on the border of weak itinerant ferromagnetism in UCoGe. *Phys Rev Lett* 99(6):067006.
16. Aoki D, et al. (2001) Coexistence of superconductivity and ferromagnetism in URhGe. *Nature* 413(6856):613–616.
17. Bernhard C, et al. (1999) Coexistence of ferromagnetism and superconductivity in the hybrid ruthenate-cuprate compound RuSr$_2$GdCu$_2$O$_8$ studied by muon spin rotation and DC magnetization. *Phys Rev B* 59(21):14099.
18. Ren Z, et al. (2009) Superconductivity induced by phosphorus doping and its co-existence with ferromagnetism in EuFe$_2$(As$_{0.7}$P$_{0.3}$)$_2$. *Phys Rev Lett* 102(13):137002.
19. Cao G, et al. (2011) Superconductivity and ferromagnetism in EuFe$_2$(As$_{1−x}$P$_x$)$_2$. *J Phys Cond Mat* 23(46):464204.
20. Ho P-C, et al. (2011) Superconductivity, magnetic order, and quadrupolar order in the filled skutterudite system Pr$_{1−x}$Nd$_x$Os$_4$Sb$_{12}$. *Phys Rev B* 83(2):024511.
21. Maple MB, Fischer Ø (1982) Magnetic superconductors. *Superconductivity in Ternary Compounds II: Topics in Current Physics*, eds Maple MB, Fischer Ø (Springer, Berlin), Vol 34, pp 1–10.
22. Kenzelmann M, et al. (2008) Coupled superconducting and magnetic order in CeCoIn$_5$. *Science* 321(5896):1652–1654.
23. Pratt DK, et al. (2009) Coexistence of competing antiferromagnetic and superconducting phases in the underdoped Ba(Fe$_{0.953}$Co$_{0.047}$)$_2$As$_2$ compound using x-ray and neutron scattering techniques. *Phys Rev Lett* 103(8):087001.
24. Khasanov R, et al. (2009) Coexistence of incommensurate magnetism and superconductivity in Fe$_{1+y}$Se$_x$Te$_{1−x}$. *Phys Rev B* 80(14):140511.
25. Mizoguchi H, et al. (2011) Coexistence of light and heavy carriers associated with superconductivity and antiferromagnetism in CeNi$_{0.8}$Bi$_2$ with a Bi square net. *Phys Rev Lett* 106(5):057002.
26. Ansari PH, Bulman JB, Huber JG, DeLong LE, Maple MB (1994) Effect of pressure on the reentrant superconductor-normal-metal phase boundaries of the (La$_{1-n}$Ce$_n$)Al$_2$ and (La$_{1−x}$Th$_x$)$_{1−n}$Ce$_n$ Kondo systems. *Phys Rev B Condens Matter* 49(6):3894–3906.
27. Wen J, Xu G, Gu G, Tranquada JM, Birgeneau RJ (2011) Interplay between magnetism and superconductivity in iron-chalcogenide superconductors: Crystal growth and characterizations. *Rep Prog Phys* 74(12):124503.
28. Bao W, et al. (2009) Tunable (deltapi, deltapi)-type antiferromagnetic order in alpha-Fe(Te,Se) superconductors. *Phys Rev Lett* 102(24):247001.
29. Liu TJ, et al. (2009) Charge-carrier localization induced by excess Fe in the superconductor Fe$_{1+y}$Te$_{1−x}$Se$_x$. *Phys Rev B* 80(17):174509.
30. Nabeshima F, Kobayashi Y, Imai Y, Tsukada I, Maeda A (2012) Effect of Co impurities on superconductivity of FeSe$_{0.4}$Te$_{0.6}$ single crystals. *Jpn J Appl Phys* 51(1):010102.
31. Zajdel P, Zubko M, Kusz J, Green MA (2010) Single crystal growth and structural properties of iron telluride doped with nickel. *Cryst Res Technol* 45(12):1316–1320.
32. Shipra R, Takeya H, Hirata K, Sundaresan A (2010) Effects of Ni and Co doping on the physical properties of tetragonal FeSe$_{0.5}$Te$_{0.5}$ superconductor. *Physica C* 470(13-14):528–532.
33. Takahashi H, Okada H, Takahashi H, Mizuguchi Y, Takano Y (2010) Electrical resistivity measurements under high pressure for FeTe$_{0.92}$. *J Phys Conf Series* 200(1):012196.
34. Chen H, Brener NE, Callaway J (1989) Electronic structure, optical and magnetic properties of fcc palladium. *Phys Rev B Condens Matter* 40(3):1443–1449.

PHYSICS

Karki et al.

35. Shinohara T, Sato T, Taniyama T (2003) Surface ferromagnetism of Pd fine particles. *Phys Rev Lett* 91(19):197201.

36. Matthias BT (1953) Superconducting compounds of nonsuperconducting elements. *Phys Rev* 90(3):487.

37. Matthias BT (1953) Transition temperatures of superconductors. *Phys Rev* 92(4):874–876.

38. Kjekshus A, Pearson WB (1965) Constitution and magnetic and electrical properties of palladium tellurides (PdTe-PdTe$_2$). *Can J Phys* 43(3):438–449.

39. Guggenheim J, Hulliger F, Muller JH (1961) PdTe$_2$, a superconductor with CdI$_2$ structure. *Helv Phys Acta* 34(V):408–410.

40. Raub Ch J, et al. (1965) The occurrence of superconductivity in sulfides, selenides, tellurides of Pt-group metals. *J Phys Chem Solids* 26(12):2051–2057.

41. Vymazalová A, Ondrus P, Drábek M (2005) Synthetic palladium tellurides, their structures and mineralogical significance. *Mineral Deposit Research: Meeting the Global Challenge* (Springer, Berlin), pp 1439–1442.

42. Karki AB, Browne DA, Stadler S, Li J, Jin R (2012) PdTe: A strongly coupled superconductor. *J Phys Condens Matter* 24(5):055701.

43. Rodriguez-Carvajal J (1993) Recent advances in magnetic structure determination by neutron powder diffraction. *Physica B* 192(1-2):55–69.

44. Ekuma CE, Lin C-H, Moreno J, Ku W, Jarrell M (2012) Why does PdTe have such a weaker superconductivity compared to FeSe? A first-principle Wannier function analysis of the electronic structure of PdTe. arXiv:1210.4512.

45. Li S, et al. (2009) First-order magnetic and structural phase transitions in Fe$_{1+y}$Se$_x$Te$_{1-x}$. *Phys Rev B* 79(5):054503.

46. Viennois R, Giannini E, van der Marel D, Černý R (2010) Effect of Fe excess on structural, magnetic and superconducting properties of single-crystalline Fe$_{1+x}$Te$_{1-y}$Se$_y$. *J Solid State Chem* 183(4):769–775.

47. Hu B, et al. (2011) Structure-property coupling in Sr$_3$(Ru$_{1-x}$Mn$_x$)$_2$O$_7$. *Phys Rev B* 84(17):174411.

48. Büscher C, et al. (1992) Ferromagnetic transition in dilute Pd-Fe alloys. *Phys Rev B Condens Matter* 46(2):983–989.

49. Crangle J (1960) Ferromagnetism in Pd-rich palladium-iron alloys. *Philos Mag* 5(52):335–342.

50. Nieuwenhuys GJ (1975) Magnetic behaviour of cobalt, iron and manganese dissolved in palladium. *Adv Phys* 24(4):515–591.

51. Schöck M, Sürgers C, Löhneysen Hv (2000) Superconducting and magnetic properties of Nb/Pd$_{1-x}$Fe$_x$/Nb triple layers. *Eur Phys B* 14(1):1–10.

52. Maple MB, Bauer ED, Zapf VS, Wosnitza J (2008) Unconventional superconductivity in novel materials. *Superconductivity: Conventional and Unconventional Superconductors*, eds Bennemann KH, Ketterson JB (Springer, Berlin), Vol 1, pp 639–762.

53. Mackenzie AP, et al. (1998) Extremely strong dependence of superconductivity on disorder in Sr$_2$RuO$_4$. *Phys Rev Lett* 80(1):161–164.

54. Subedi A, Zhang L, Singh DJ, Du MH (2008) Density functional study of FeS, FeSe, and FeTe: Electronic structure, magnetism, phonons, and superconductivity. *Phys Rev B* 78(13):134514.

Karki et al.